Monthly Notices of the ROYAL ASTRONOMICAL SOCIETY

MNRAS **452,** 1316–1327 (2015) doi:10.1093/mnras/stv1383

3D plausible orbital stability close to asteroid (216) Kleopatra

T. G. G. Chanut,★ O. C. Winter, A. Amarante and N. C. S. Araújo

Univ. Estadual Paulista – UNESP, Grupo de Dinâmica Orbital & Planetologia, Guaratinguetá, CEP 12516-410, SP, Brazil

Accepted 2015 June 19. Received 2015 June 16; in original form 2014 November 28

ABSTRACT

Recent data processing showed the existence of a difference that can reach 25 per cent for the dimensions of asteroid (216) Kleopatra between the radar observations and the light curves. We rebuild the shape of (216) Kleopatra from these new data applying a correction's factor of the size of 1.15 and estimate certain physical features by using the polyhedral model method. In our computations, we use a code that avoids singularities from the line integrals of a homogeneous arbitrary shaped polyhedral source. Then, we find the location of the equilibrium points through the pseudo-potential energy and zero-velocity curves. The behaviour of the zero-velocity curves differ substantially if we apply a scale size of 1.15 relative to the original shape of (216) Kleopatra. Taking the rotation of asteroid (216) Kleopatra into consideration, the aim of this work is to analyse the stability against impact and the dynamics of numerical simulations of 3D initially equatorial and polar orbits near the body. As results, we show that the minimum radii are more suited for the stability against impact. We find also that the minimum radius for direct, equatorial circular orbits that cannot impact with (216) Kleopatra surface is 300 km and the lower limit on radius for polar circular orbits is 240 km. Stable orbits occur at 280 km for equatorial circular orbits despite significant perturbations of its orbit. Moreover, as the orbits suffer less perturbations due to the irregular gravitational potential of (216) Kleopatra in the elliptic case, the most significant result of the analysis is that stable orbits exist at a periapsis radius of 250 km for initial eccentricities $e_i = 0.2$ in both cases. Finally, the polar orbits with eccentricities ranging between 0.1 and 0.2 appear to be more stable.

Key words: gravitation – methods: numerical – celestial mechanics – minor planets – asteroids: individual: (216) Kleopatra.

1 INTRODUCTION

The most intriguing main-belt asteroid (216) Kleopatra received a particular attention during the last three decades. Ostro, Campbell & Shapiro (1985) classified (216) Kleopatra as an M-type asteroid. M-type is basically composed by NiFe metal. Its significant brightness variation (up to 1.2 mag) over a short spin period fixed at 5.385 h (Magnusson 1990) has puzzled researchers. Ostro et al. (2000) performed radar observations from Arecibo observatory and reconstructed a three-dimensional shape similar to a dog-bone with dimensions of 217 × 94 × 81 km and an equivalent diameter of 108.5 ± 15 km, which has been used ever since. They found from the reflectivity, a surface bulk density no less than 3.5 g cm^{-3}, consistent with a metallic surface with a porosity of <60 per cent. Note that the shape model provides a volume of 7.09×10^5 km^3. Nevertheless, spectroscopic measurements from the *Infrared Astronomical Satellite* (*IRAS*) have found a larger diameter (Tedesco et al. 2002) showing that the size uncertainty was up 25 per cent. Thermals modelling of mid-infrared radiometry like STM (Lebofsky& Spencer 1989) and NEATM (Harris 1998) also were used. In 2008 September, leveraging the Kleopatra's passage in opposition at 1.23 au from Earth, Ryan & Woodward (2010) presented new measurements of the Kleopatra diameter from 119.55 ± 3.21 km (STM) until 140.74 ± 7.78 km (NEATM) using the NASA *Spitzer* space telescope. Also, Descamps et al. (2011) calculated the mass as $4.64 \times 10^{18} \pm 0.02$ kg from the mutual gravitational interaction between (216) Kleopatra and its two satellites using a near-infrared adaptive optics with the W.M. Keck II telescope combined with the *Spitzer*. Furthermore, they established the bulk density as 3.6 ± 0.4 g cm^{-3} based in a mean porosity of lunar soil of 44 per cent (Scott 1963). With this mass and density, the size of Descamps et al. (2011) is 1.22 larger than the size of Ostro et al. (2000). However, more recent works of mechanical properties of lunar soil (Mitchell et al. 1972) showed that Apollo 15 data from station 8 have had best estimates of porosity ranging 35–38 per cent and the soil density evidently increases fairly rapidly with depth. So a bulk density of (216) Kleopatra upper than 4.0 g cm^{-3} is

★ E-mail: thierry@feg.unesp.br

expected. In this way, Carry (2012) did a detailed work about the density of asteroids and showed that the plausible density of (216) Kleopatra is $4.27 \pm 0.86\,\mathrm{g\,cm^{-3}}$. With the diameter estimated close to 127.50 km, the size is 1.15 larger than the size of Ostro et al. (2000). These papers indicate that the size of asteroid (216) Kleopatra is not well understood. The study of the dynamics around (216) Kleopatra claims the attention because its puzzling dog bone shape can exhibit some trajectories strongly unstable and chaotic motion near the surface. Thus, a planning for a mission to reach (216) Kleopatra become necessary to understand its shape and high density. From the NASA Ephemerides, the best Kleopatra's passage in opposition at 1.15 au from Earth has happened in 2013 September and is expected only in 2027 November. Therefore, the configuration at 1.23 au from Earth encountered in 2008 may occur in 2022 September.

On the other hand, we need models each time more efficient for the planning of future missions around asteroids with these characteristics. The polyhedral method describes the gravitational field of a constant density polyhedron and is effective to estimate the gravitational field around a specific asteroid (Rossi et al. 1999). Previous studies used the polyhedral method (Werner & Scheeres 1997; Tsoulis & Petrović 2001) to evaluate the actual dynamical environments around 433 Eros and 25143 Itokawa (Scheeres, Williams & Miller 2000; Scheeres et al. 2006; Chanut, Winter & Tshuchida 2014). Regarding (216) Kleopatra, Yu & Baoyin (2012, 2013) studied the stability close to the equilibrium points. They have chosen the mass and density of Descamps et al. (2011) and the size of Ostro et al. (2000). If we choose this size, the density should be $6.5\,\mathrm{g\,cm^{-3}}$ and the equilibrium points are farther away from the surface as shown Hirabayashi & Scheeres (2014). Our interest for (216) Kleopatra is due to the fact that a correction factor of the size becomes necessary for further analyses.

In this paper, we evaluate the full gravity tensor of (216) Kleopatra using the improved method implemented by Tsoulis (2012). The study of the stability of equatorial and polar orbits in the vicinity of the body is done taking into account the correction of the size of 1.15 applied to the more plausible density. First, the general properties of (216) Kleopatra are discussed in Section 2. In Section 3, we present the full gravity tensor of the polyhedral model. The equations of motion and the conserved quantity are discussed in Section 4 as well as the stability against impact in both orbital cases. We also find the exact location of the seven equilibrium points and their stability. The dynamics of equatorial and polar orbits close to (216) Kleopatra is investigated through numerical simulations and the results are presented in Section 5. Then, we discuss and conclude in Section 6.

2 COMPUTED PHYSICAL PROPERTIES FROM THE SHAPE OF (216) KLEOPATRA

In 1999, Ostro et al. (2000) have made observations via the Arecibo radar Observatory allowing us to generate the data of the shape of (216) Kleopatra. We choose the data set of EAR-A-5-DDR-RADARSHAPE-MODELS-V2.0 from NASA Planetary Data System (2004) to build a polyhedral model with 2048 vertices and 4092 faces. From orbital measurements of (216) Kleopatra's satellites, taking advantage of its passage in opposition at 1.23 au, the total mass of the asteroid was set as 4.64×10^{18} kg (Descamps et al. 2011). For the bulk density, we adopt the value of $4.27\,\mathrm{g\,cm^{-3}}$ established by Carry (2012). Based on these measurements, the new dimensions of (216) Kleopatra are $252 \times 108 \times 96$ km and the total volume is $1.0867 \times 10^6\,\mathrm{km^3}$. Fig. 1 illustrate the polyhedron shape

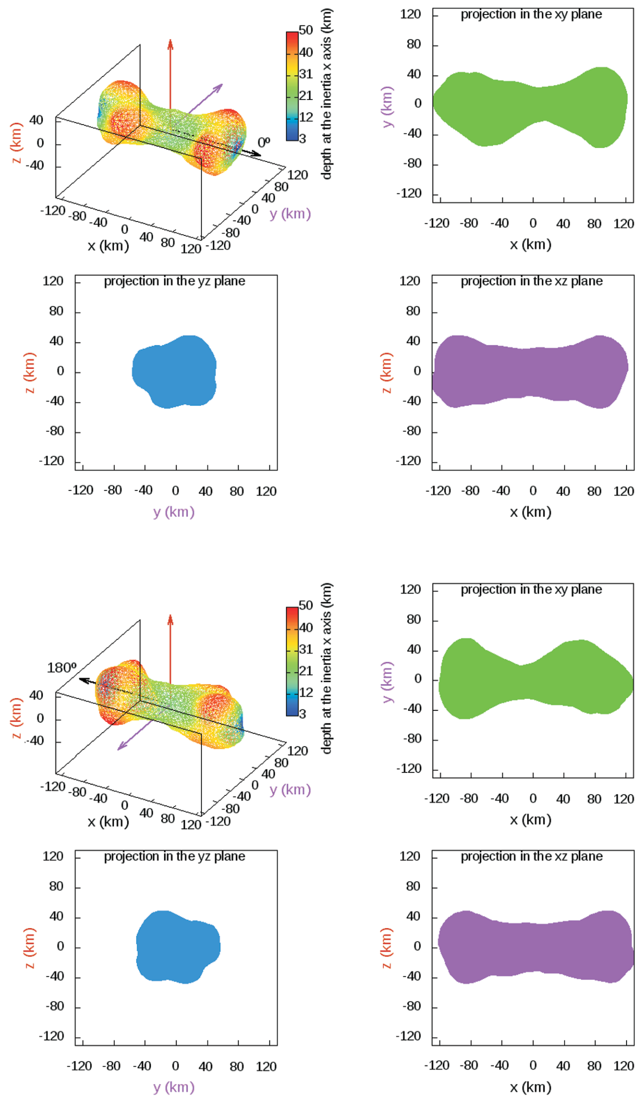

Figure 1. Polyhedron shape model in 3D of asteroid (216) Kleopatra viewed from two opposite perspectives. The projections are in the *xoy*, *xoz* and *yoz* planes, respectively. The shape was built with 4092 faces and the colour code gives the distance from the inertia axis *x* in km.

model 3D of (216) Kleopatra and its projections viewed from two opposite directions. The colour code gives the depth at the major axis *x*. The red colour highlights the dog bone shape or dumbbell. The overall dimensions of the asteroid shape in each of the principal directions are

$$
\begin{aligned}
-130.1513 &\le x \le 122.4044\,\mathrm{km},\\
-56.7755 &\le y \le 51.1957\,\mathrm{km},\\
-47.1270 &\le z \le 49.4557\,\mathrm{km}.
\end{aligned}
\tag{1}
$$

We use a fast and effective algorithm (Mirtich 1996) to calculate the polyhedral mass properties of (216) Kleopatra and then, we find the body-fixed coordinate frame with origin at the body centre of mass, and aligned with the principal axes of inertia of the asteroid. Thus, using this algorithm we also find the values of the moments of the principal axes of inertia, respectively, J_x, J_y and J_z:

$$J_x = 4.0543 \times 10^{21}\ \mathrm{kg\,km}^2,$$
$$J_y = 2.7672 \times 10^{22}\ \mathrm{kg\,km}^2,$$
$$J_z = 2.7875 \times 10^{22}\ \mathrm{kg\,km}^2. \tag{2}$$

The values do not agree with those found by Yu & Baoyin (2012), since the volume of (216) Kleopatra was determined with an inaccuracy associated with the radar's measurements of up to 25 per cent (Descamps et al. 2011).

From the moments of inertia (Dobrovolskis 1996), we can solve for the ellipsoid and we find a body with semimajor axes of 166.5659 × 47.8954 × 45.5507 km, which are not so close to the overall dimensions of the body given in equation (1). This is mainly due to its shape in 'dog bone or dumbbell' shown in Fig. 1. Directly related to moments of inertia are the second-degree and -order gravity coefficients. These are computed to be (Werner & Scheeres 1997)

$$C_{20}R_0^2 = -2.5888 \times 10^3\ \mathrm{km}^2,$$
$$C_{22}R_0^2 = \ \ 1.2725 \times 10^3\ \mathrm{km}^2, \tag{3}$$

where R_0 is the arbitrary normalization radius.

A measure of the asteroids shape and gravity field is defined in Hu & Scheeres (2004) as

$$\sigma = \frac{J_y - J_x}{J_z - J_x} = -\frac{4C_{22}}{C_{20} - 2C_{22}}. \tag{4}$$

For (216) Kleopatra, $\sigma = 0.9915$. A body with $\sigma = 1$ has a prolate inertia matrix, while one with $\sigma = 0$ has an oblate matrix, thus we see that (216) Kleopatra is very close to having a prolate shape index, that is compatible with Fig. 1.

3 FULL GRAVITY TENSOR OF THE POLYHEDRAL MODEL

Tsoulis & Petrović (2001) present a mathematical approach that overcomes the singularities, that we will define in this section, and enables the line integral formalism to be applied everywhere in space. The closed formulas for the potential, the gravitation vector, and the tensor of the second-order derivatives, are respectively:

$$U = \frac{G\rho}{2}\sum_{p=1}^{n}\sigma_p h_p\left[\sum_{q=1}^{m}\sigma_{pq}h_{pq}LN_{pq} + h_p\sum_{q=1}^{m}\sigma_{pq}AN_{pq} + \sin g_{Ap}\right], \tag{5}$$

$$U_{x_i} = G\rho\sum_{p=1}^{n}\cos(\boldsymbol{N}_p,\boldsymbol{e}_i)\left[\sum_{q=1}^{m}\sigma_{pq}h_{pq}LN_{pq} + h_p\sum_{q=1}^{m}\sigma_{pq}AN_{pq} + \sin g_{Ap}\right] \quad (i = 1, 2, 3), \tag{6}$$

$$U_{x_ix_j} = G\rho\sum_{p=1}^{n}\cos(\boldsymbol{N}_p,\boldsymbol{e}_i)\left[\sum_{q=1}^{m}\cos(\boldsymbol{n}_{pq},\boldsymbol{e}_j)LN_{pq} + \sigma_p\cos(\boldsymbol{N}_p,\boldsymbol{e}_i)\sum_{q=1}^{m}\sigma_{pq}AN_{pq} + \sin g_{B_{pj}}\right](i, j = 1, 2, 3). \tag{7}$$

Here, the additional parametrization refers to the plane defined by each polygonal surface S_{p}. Thus, subscript q stands for the polyhedral segments, and it is running from one to m for each face p, with m denoting the variable number of maximum segments building every face. The value $\boldsymbol{n}_{pq}$ is the normal vector of segment q that lies on the plane of polygon S_{p} and is pointing, per definition, outside the closed polygonal surface S_{p}. A critical information for each face is the relative position of the projection P' of the computation point P on the plane of each face with respect to S_{p}. If $\boldsymbol{n}_{pq}$ points to the half-plane that contains P', then $\sigma_{pq} = -1$; if it points to the other half-plane, it holds that $\sigma_{pq} = +1$. The value h_{pq} denotes the positive distance between P' and the line of each segment, whereas $\cos(\boldsymbol{n}_{pq}, \boldsymbol{e}_j)$ is the direction cosine between $\boldsymbol{n}_{pq}$ and the unit vector $\boldsymbol{e}_j$) of the unit vector triad situated at P. Quantities LN_{pq} and AN_{pq} are abbreviations of the following transcendental expressions:

$$LN_{pq} = \ln\frac{s_{2pq} + l_{2pq}}{s_{1pq} + l_{1pq}} \tag{8}$$

and

$$AN_{pq} = \arctan\frac{h_p s_{2pq}}{h_{pq}l_{2pq}} - \arctan\frac{h_p s_{1pq}}{h_{pq}l_{1pq}}, \tag{9}$$

where l_{1pq} and l_{2pq} are the 3D distances between P and the end points of segment pq (e.g. fig. 1 of Tsoulis & Petrović 2001). With P'' being the origin of a 1D local coordinate system defined on the line of segment pq, s_{1pq} and s_{2pq} are the 1D distances between P'' and the two segment end points. In these definitions, subscript 1 always stands for the end, and subscript 2 is for the beginning of the corresponding segment vector (Tsoulis 1999). Finally, the terms sing_{Ap} and $\mathrm{sing}_{B_{pj}}$ are the singularity terms that appear for specific locations of P' with respect to the polygonal line G_{p} when one attempts to apply the divergence theorem of Gauss for these cases. Tsoulis & Petrović (2001) showed the values of the three cases when (a) P' lie inside S_{p}, (b) P' is located on G_{p} but not at any of its vertices and (c) P' is located at one of G_{p}'s vertices.

We computed the program in FORTRAN (Tsoulis 2012) applied to (216) Kleopatra. The results for the three planes of the distribution of the gravitational potential are shown in Fig. 2. Contour maps of the surfaces are used to show the equipotential lines.

The equipotential surfaces are displayed for three values in Fig. 3. Figs 2 and 3 indicate that more simple models, as spherical, that corresponds to a point mass, or ellipsoidal with second-degree and -order gravity coefficients, would not represent so well the gravitational potential of (216) Kleopatra at a distance smaller than 200 km from the centre of mass. Thus, simple shape models like ellipsoid could be chosen to analyse the dynamics of orbits around (216) Kleopatra with periapsis radii larger than 200 km. Close to the body, it becomes necessary to use the polyhedral model for a more accurate calculations.

4 EQUATIONS OF MOTION AND CONSERVED QUANTITIES

4.1 Equations of motion

In fact, the radiation pressure from the Sun has a constant direction and magnitude at a given distance of the asteroid from the Sun. Actually, the effect of this force becomes more pronounced as the spacecraft flies farther away from the asteroid. As the effect of the solar gravity becomes relevant as the distance of the spacecraft from the asteroid increases and is equal to the asteroid gravity at the Hill sphere. However, the influence of solar radiation pressure

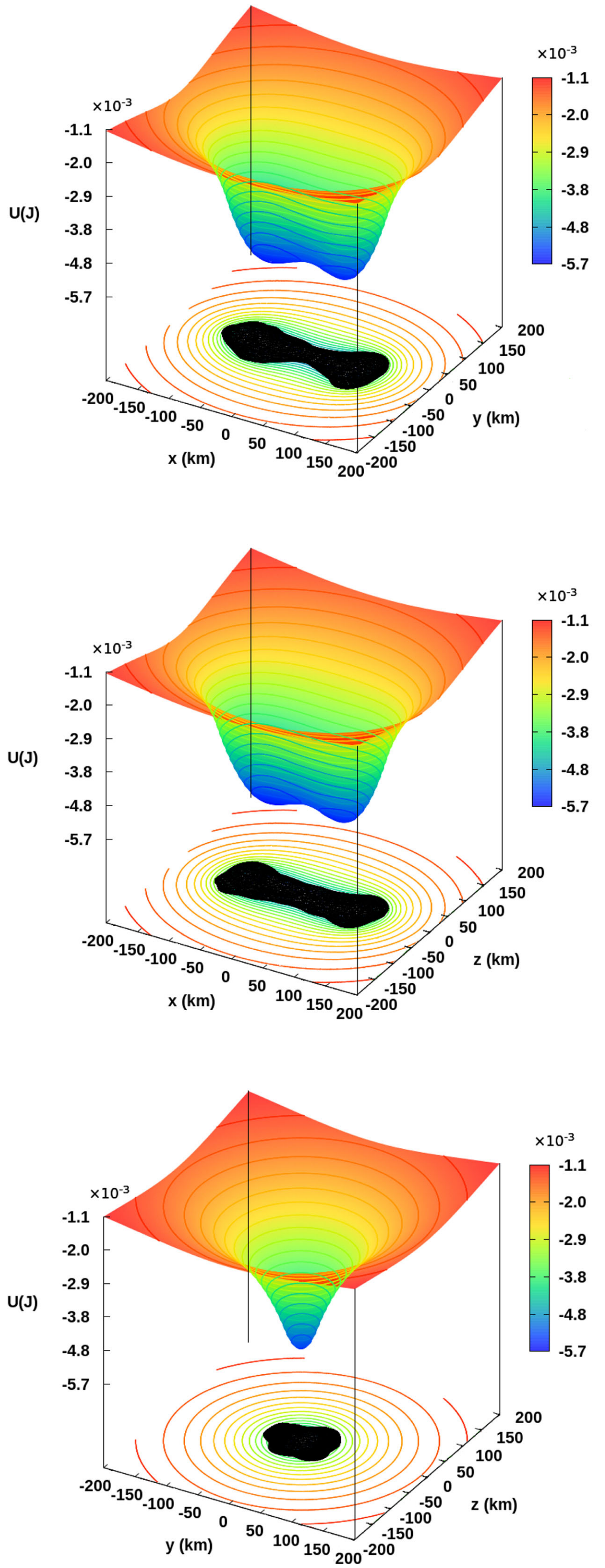

Figure 2. Gravitational potential of asteroid (216) Kleopatra in the *xoy*, *xoz* and *yoz* planes, respectively. The colour code gives the intensity of the potential in km^2 s^{-2}

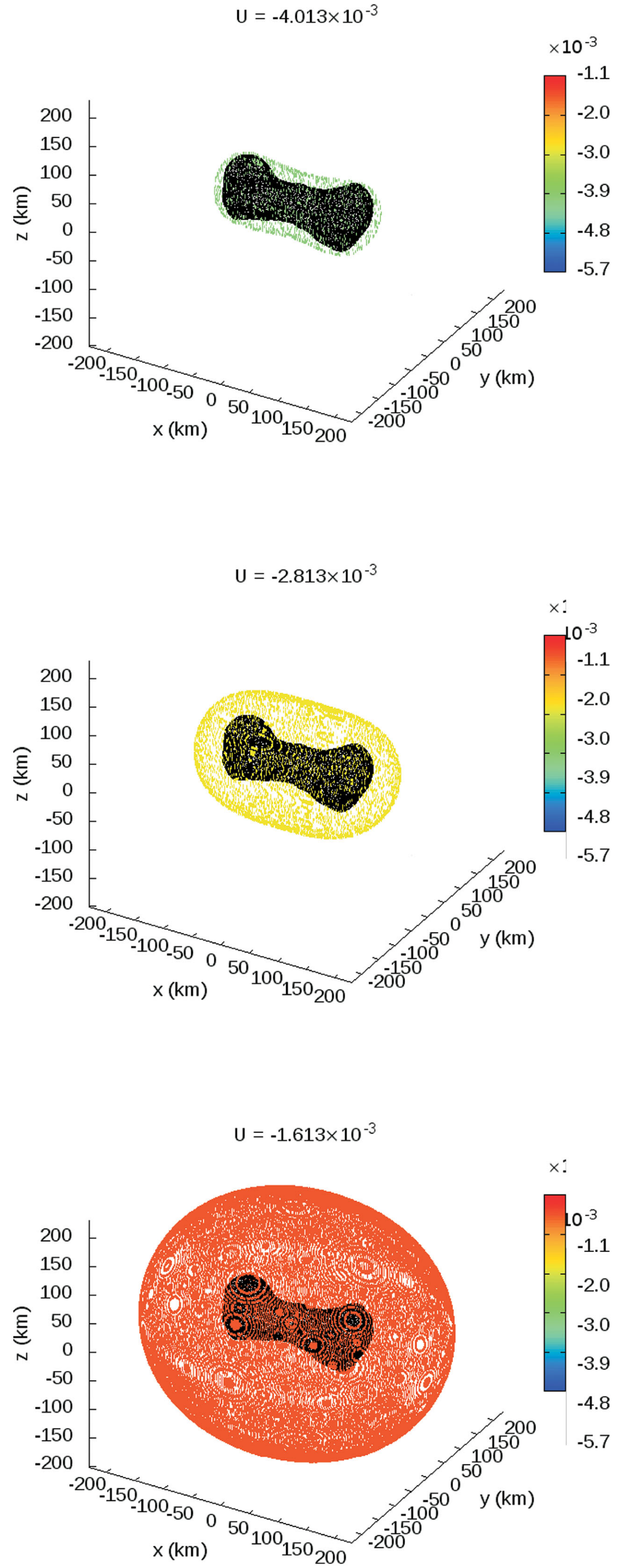

Figure 3. Equipotential surfaces of asteroid (216) Kleopatra for three values of potential. The colour code gives the intensity of the potential in km^2 s^{-2}

can lead to both unstable and stable spacecraft orbits near bodies with diameter smaller than few kilometres (Hussmann et al. 2012). In the present case, the magnitude of the radiation pressure is at the most one millionth of the gravitational force, and as discussed by Scheeres et al. (2000) for asteroid (433) Eros, the orbital motion in the vicinity of bodies as (216) Kleopatra is dominated by its own gravitational field, which allows us to neglect any solar effects and gravitational pull from remaining bodies in this paper.

For the spin period of (216) Kleopatra, we set the value found by Magnusson (1990) of 5.385 *h*. The spin rate of the asteroid is denoted as ω. Thus, in the body-fixed reference frame (Scheeres et al. 2000), the equations of motion are

$$\ddot{x} - 2\omega\dot{y} = \omega^2 x + U_x, \tag{10}$$

$$\ddot{y} + 2\omega\dot{x} = \omega^2 y + U_y, \tag{11}$$

$$\ddot{z} = U_z, \tag{12}$$

where U_x, U_y and U_z are the first-order partial derivatives of the potential. Because these equations are time invariant, an additional integral of motion called the Jacobi constant exists. The Jacobi constant C is explicitly calculated as (Scheeres et al. 1996)

$$C = V(x, y, z) - T_{\mathrm{E}} \tag{13}$$

where

$$V(x, y, z) = \frac{1}{2}\omega^2(x^2 + y^2) + U(x, y, z) \tag{14}$$

is the modified potential and

$$T_{\mathrm{E}} = \frac{1}{2}(\dot{x}^2 + \dot{y}^2 + \dot{z}^2) \tag{15}$$

is the kinetic energy of the particle with respect to the rotating asteroid.

4.2 Zero-velocity surfaces and equilibria

Zero-velocity surfaces, defined using the Jacobi integral, provide concrete information regarding the possible motion of a particle. Since $T_{\mathrm{E}} \geq 0$, it is possible to define an inequality

$$V(x, y, z) \geq C, \tag{16}$$

that partitions the x, y, z space into regions where the particle is allowed to be found and where it cannot be found, given a specific value for C. Note that $V(x, y, z) \geq 0$ over the entire space. Thus, if $C < 0$, the inequality is identically satisfied and there are no a priori constraints on where the particle may be found. If $C > 0$, there will be regions of space where the inequality is violated, and hence where no particle may travel. When these forbidden regions separate space into disjoint regions, a particle can never travel between these regions. The general situation is discussed more fully in Scheeres (1994), where the central body is assumed to be a three axial ellipsoid. Zero-velocity surfaces are defined by

$$V(x, y, z) = C, \tag{17}$$

and Fig. 4 shows the projections of the zero-velocity surfaces on to the $z = 0$ plane. As the value of the Jacobi constant C is varied, the surfaces change. At critical values of C the surfaces intersect or close in upon themselves at points in the x–y–z space, usually called equilibrium points. The surfaces are all evaluated close to the critical values of C, and Fig. 4 indicates the location of the equilibrium points in the equatorial plane. In the three-dimensional x–y–z space, Yu & Baoyin (2012) showed the zero-velocity surfaces of (216) Kleopatra with different values of the Jacobi constant. However, they assigned the size of Ostro et al. (2000) with a density not compatible with the mass (Descamps et al. 2011). Thus, we apply a correction's factor of 1.15 of the size of (216) Kleopatra displayed on the right-hand side of Fig. 5, while on the left-hand side the size of Ostro et al. (2000) without any correction is applied. If $C = C1$, the zero-velocity surface consists of two branches or branching trajectories on the left-hand side of the figure. The inner one clings to around the asteroid and the outer one is cylindrical. Here, the allowable region is divided into two parts: orbits initialized in the outer branch will never approach the asteroid, whereas those initialized in the inner branch will end up colliding with the asteroid. These two branches begin to connect on the right-hand side of the figure; the allowable regions merge into one, and the outer and inner orbits move to the side through the neck area. The zero-velocity surface splits into two branches on the same side of the figure when $C = C2$. The upper branch and lower branch are dividing the forbidden region into two parts. This indicates that all orbits near the equatorial plane are probable at this time ($C \geq C2$), which does not occur on the left-hand side of the figure.

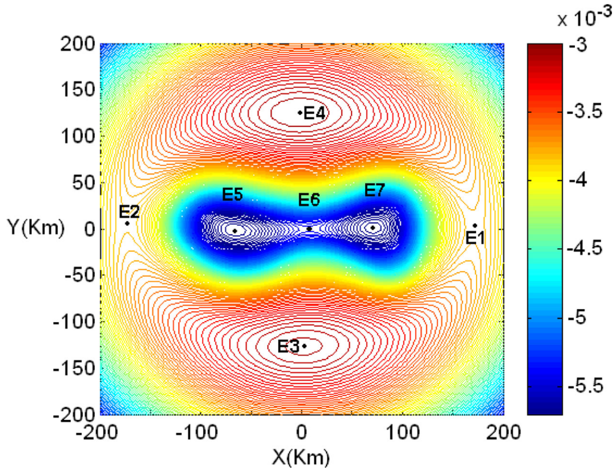

Figure 4. Zero-velocity curves and equilibrium points of asteroid (216) Kleopatra in the *xoy* plane. The colour code gives the intensity of the Jacobi constant in $\mathrm{km}^2\ \mathrm{s}^{-2}$. The equilibrium points outside the body are indicated by *E*1, *E*2, *E*3 and *E*4, and inside it by *E*5, *E*6 and *E*7.

To find the exact location of the equilibrium points, we make

$$\nabla V(x, y, z) = 0, \tag{18}$$

and the results are shown in Table 1 including the energy value C for each point. Due to (216) Kleopatra irregular shape, there is no symmetry between the saddle points and the centre points. As showed by Yu & Baoyin (2012), all the four equilibrium points outside (216) Kleopatra ($E1 - E4$) are unstable. The state equations in the neighbourhood of the equilibrium points can be summarized as

$$\dot{\boldsymbol{\varepsilon}} = \mathbf{A}\boldsymbol{\varepsilon}, \tag{19}$$

where $\boldsymbol{\varepsilon}$ is the state variable and $\mathbf{A}$ is the coefficient matrix of the linearized system. The eigenvalues of matrix $\mathbf{A}$ are obtained by solving $\det(\mathbf{A} - \lambda I) = 0$. Furthermore, for the non-degenerate and non-resonant equilibrium points in the potential field of a celestial

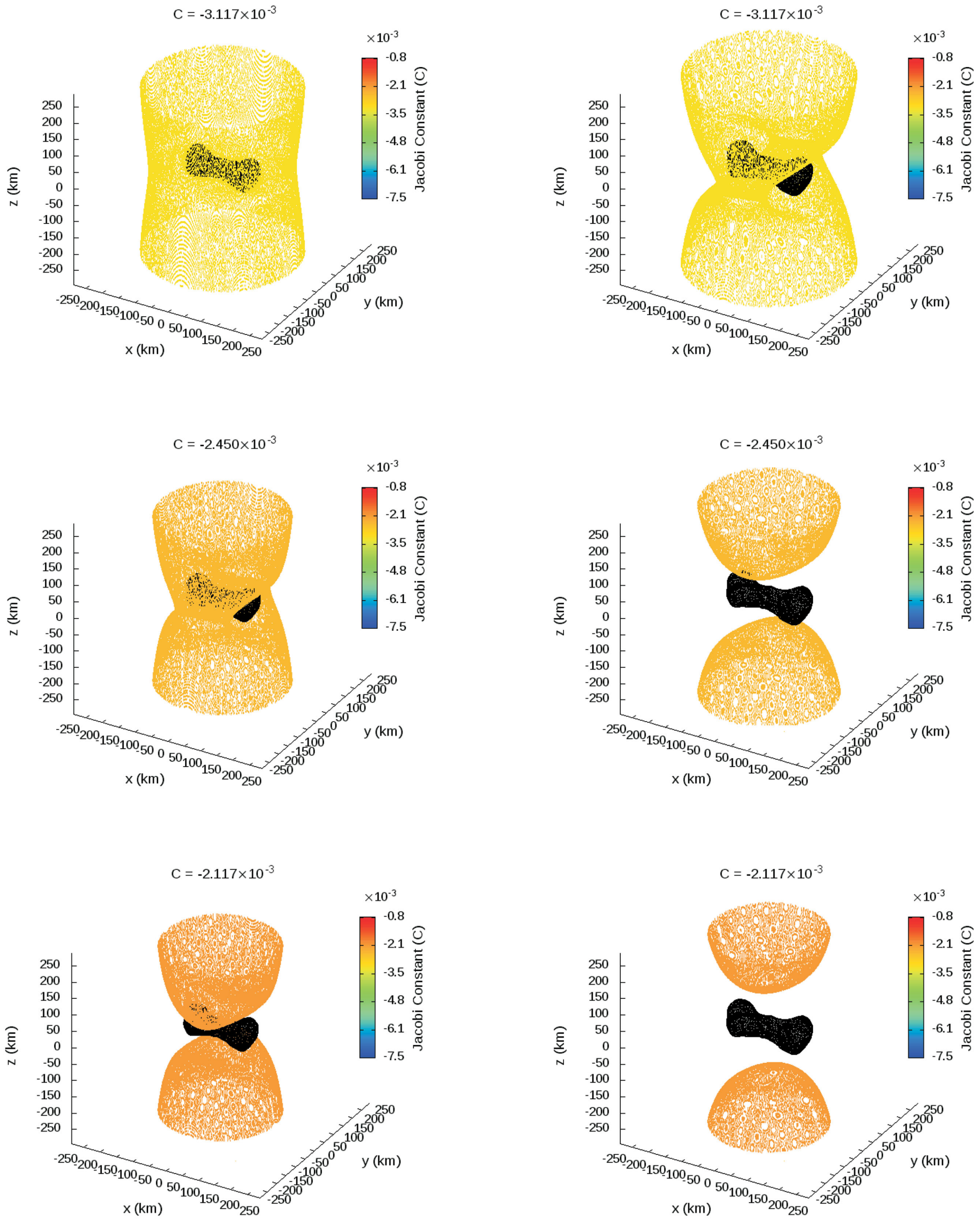

Figure 5. Zero-velocity surfaces with different values of the Jacobi Integral C (in km^2 s^{-2}). The scale size correction is not applied on the left-hand side of the figure, and on the right-hand side a scale size correction of 1.15 is applied. $C = C_1 = -3.117 \times 10^{-3}$ (top), $C = C_2 = -2.450 \times 10^{-3}$ (middle) $C = C_3 = -2.117 \times 10^{-3}$ (bottom).

Table 1. Locations of equilibrium points, their respective Jacobi constant C values.

Equilibrium point	x(km)	y(km)	z(km)	C(km^2 s^{-2})
$E1$	171.6276	2.7349	1.2126	− 3.730 942e−03
$E2$	− 173.4952	5.9213	− 0.2166	− 3.754 823e−03
$E3$	2.2384	− 126.5944	0.2771	− 2.993 243e−03
$E4$	− 1.4974	125.0958	− 0.5483	− 2.975 183e−03
$E5$	− 66.0664	− 1.3983	− 0.2098	− 5.879 423e−03
$E6$	7.4907	− 0.2146	− 0.3680	− 5.427 423e−03
$E7$	71.1619	0.9078	− 0.8989	− 5.846 401e−03

Table 2. Eigenvalues of the coefficient matrix of the inner equilibrium points and their stability.

Eigenvalues ($\times 10^{-3}$)	$E5$	$E6$	$E7$
λ_1	0.651 049i	0.533 895	0.723 990i
λ_2	− 0.65 1049i	− 0.533 895	− 0.723 990i
λ_3	1.437 286i	1.627 363i	1.426 237i
λ_4	− 1.437 286i	− 1.627 363i	− 1.426 237i
λ_5	1.229 475i	1.279 842i	1.201 228i
λ_6	− 1.229 475i	− 1.279 842i	− 1.201 228i
Stability	LS	U	LS

body, Jiang et al. (2014) presented several cases of eigenvalues and the resulting stability. In their classification, only the purely imaginary eigenvalues leads to a linear stability of the equilibrium points. We present the eigenvalues of matrix **A** for the inner points of (216) Kleopatra in Table 2. The equilibrium point $E6$ located at the centre of the body is unstable while the other two inner equilibrium points $E5$ and $E7$ are both linearly stable.

4.3 Stability against impact

Assuming a case in which the motion occurs only in the plane, to ensure stability against impact, we must choose the initial orbital conditions such that the spacecraft position resides in the outer portion of the closed zero-velocity curve. Then we have explicitly that a spacecraft in orbit in the outer region with the appropriate Jacobi integral value can never, under gravitational dynamics alone, impact on to the asteroid surface. That would be when the value of the Jacobi integral is less than or equal to $J_0 = -3.7548 \times 10^{-3}$ km^2 s^{-2} directly found from (216) Kleopatra shape model. This provides a simple check for whether or not the spacecraft might impact with the surface at some point in the future. This relation can be expressed in terms of initial osculating elements for an assumed direct, equatorial orbit specified by its periapsis radius r_p, eccentricity e and initial longitude λ in the body-fixed frame (Scheeres et al. 2000):

$$\frac{-\mu(1+e)}{2r_{\rm p}} + \omega_K\sqrt{\mu r_{\rm p}(1+e)} + U(r = r_{\rm p}, \lambda) + J_0 = 0, \qquad (20)$$

where the gravitational potential $U(r, \lambda)$ is evaluated from the actual gravity field, $\omega_K = 3.2411 \times 10^{-4}$ rad s^{-1} and $\mu = 0.309\,608$ km^3 s^{-2}.

Fig. 6 shows the planar stability against impact including the full effect of the irregular gravity field) in terms of initial periapsis radius and eccentricity for an equatorial orbit around (216) Kleopatra. As the gravitational field is very irregular close to the body, the sign of expression (19) can change several times before becoming always positive. The green line at the top of the figure represents the maximum periapsis radius where this change of sign occurs. Initial orbits to the left of this line may or not impact with (216) Kleopatra at some point in the future; orbits to the right of this line will not impact with (216) Kleopatra. The blue line represents the

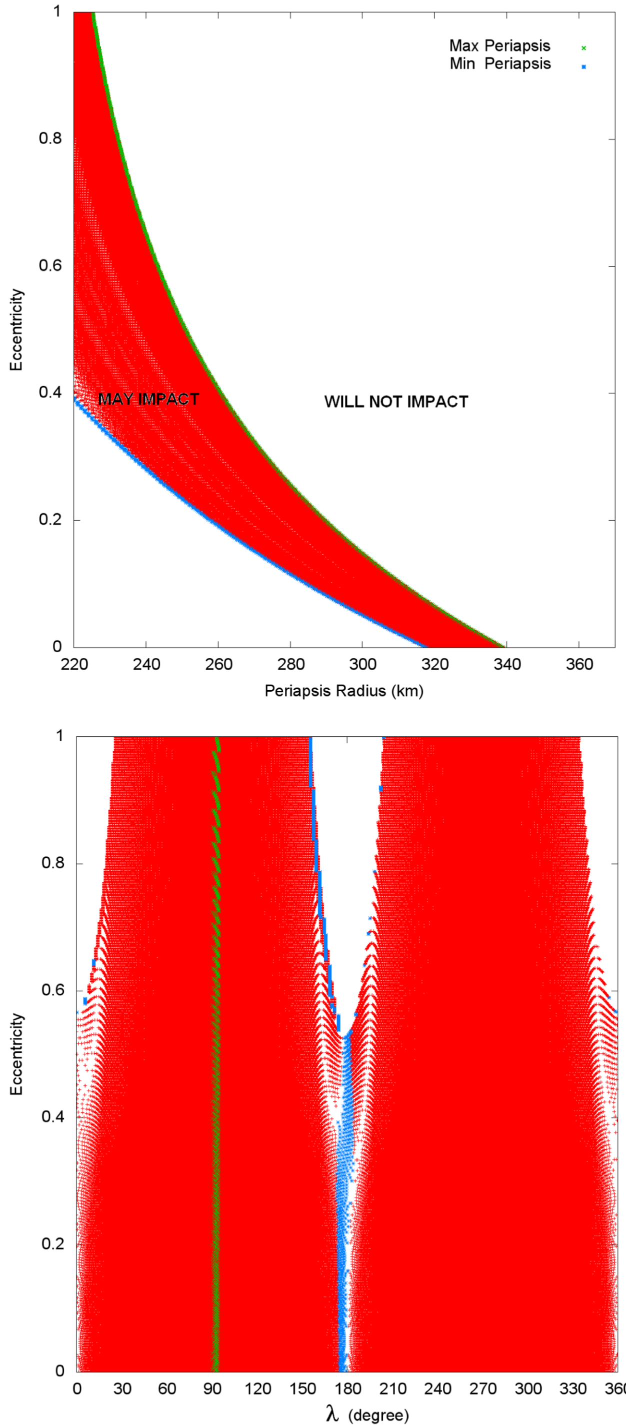

Figure 6. Stability against impact curves for equatorial, direct orbits, derived from equation (20). On the top of the figure, the green line represents the maximum periapsis radius where changes the sign of equation (19) and the blue line represents the minimum periapsis radius. The bottom of the figure represents the latitude $\lambda \in (0°, 360°)$ where it occurs.

minimum periapsis radius where the first change of sign occurs. The bottom of the figure shows the longitude where the maximum and minimum periapsis radii are located. The maximum periapsis radii are concentrated on 90° while the minimum periapsis radii are found around 180°. It means that orbits starting from a longitude of 180° are less likely to collide with (216) Kleopatra.

Regarding a polar orbit specified by its periapsis radius r_p, eccentricity e and initial longitude λ in the body-fixed frame, we have

$$\frac{-\mu(1+e)}{2r_p} + U(r = r_p, \lambda) + J_0 = 0. \tag{21}$$

Analytically, there does not exist a separating line for the stability against impact of the polar orbits around (216) Kleopatra. Indeed, the expression (20) never cancels and is always negative. Thus, the polar orbits seem to be all unstable close to body.

5 DYNAMICS EVOLUTION CLOSE TO (216) KLEOPATRA

5.1 Numerical simulations

Our goal is to numerically test and expand the evolution of the dynamics of equatorial and polar direct orbits, taking into account the 3D gravitational perturbation around (216) Kleopatra. So as done in the previous section we adopt the full potential tensor method implemented by Tsoulis (2012) to calculate the gravitational field of the equations of motion (equations 4–6) in the body-fixed reference frame. The Bulirsch–Stoer numerical algorithm was used to integrate the equations. The initial conditions of the spacecraft are placed in the periapsis radius of the equatorial and polar planes ($z = 0$ and $x = 0$, respectively) for different values of $\lambda \in (0°, 360°)$. We consider also two types of polar orbits. One in which the spacecraft rotates in anticlockwise direction and the other in clockwise direction. The interval between each initial value of λ is 30°, being that the initial velocities are given from the two-body problem in the body-fixed reference frame. The initial periapsis radii vary from 220 up to 300 km with interval of 10 km for the equatorial orbits, and from 100 up to 280 km with interval of 20 km for the polar orbits. The initial eccentricities of the spacecraft's orbit vary from 0 up to 0.8 with interval of 0.1. When the path of the spacecraft passes the boundaries of the ellipsoid approximation with semimajor axes (130 × 60 × 50 km), the integration is stopped and we consider that the spacecraft impacted with the asteroid. The integration's time is 1000 h (over 40 d) to determinate the final destiny of the orbits (Scheeres, Miller & Yeomans 2003).

5.2 Results

Two-dimensional analytical limits of stability against the impact on the equatorial plane of (216) Kleopatra were shown in the previous section. Our interest in the present section is to show the behaviour of orbits launched with initial conditions compatible with Fig. 6, but in which case we consider the full gravitational potential in the three-dimensional model, and we followed the trajectories in the 3D space to verify the outcome. The trajectories are made from various initial longitudes in the equatorial plane. We chose four of them which occur, in principle, the highest and lowest values of the potential and we show them in Fig. 7. We see that the results have a similar behaviour with the curves of Fig. 6. However, the periapsis radii that impact with the asteroid are mostly below the blue line. Such case also occurred with (433) Eros (Chanut et al. 2014). Nevertheless, below 220 km, the orbits are unstable independently of the initial eccentricity. We check all the longitudes, and we find that the limit radius for direct, initially equatorial circular orbits that cannot impact with (216) Kleopatra surface is 300 km. Moreover, orbits with initial $\lambda = \pi$ appear to be less subject to collision. Compatible results with those of the bottom of Fig. 6. We are now interested in finding out what occurs numerically with the polar orbits close to (216) Kleopatra. The number of initial conditions that impact or not with the body for four periapsis radius with eccentricities up to 0.3 is shown in Table 3. Comparing the results in general between the polar anticlockwise orbits and the polar clockwise orbits, we note that the polar anticlockwise orbits are a slightly more stable when the periapsis radius pulls away from (216) Kleopatra up to <220 km. In the circular case, the collisions dominate up to 180 km. However, at this periapsis distance, the number of initial conditions that do not collide with (216) Kleopatra is much higher with an initial eccentricity. Thus from 220 km, the initial conditions, that do not collide, totally dominate even with eccentricities close or equal to zero. Therefore, Table 3 shows numerically that polar orbits have a lower limit on periapsis radius that, if violated, soon led to unstable (colliding) orbital motion. The lower limit for eccentric polar orbits around (216) Kleopatra seems to be 220 km and consequently 240 km for circular polar orbits.

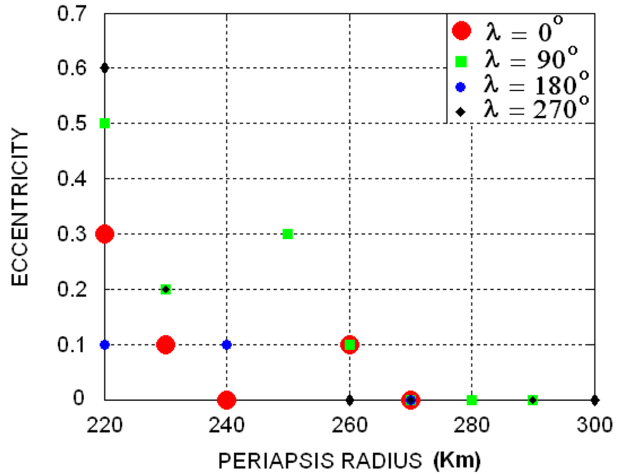

Figure 7. Maximal eccentricity of the initial equatorial orbit of the particles that have impacted with (216) Kleopatra according to their periapsis radius. We show this relation for four initial longitudes λ.

Taking into account only those trajectories which do not collide with the body, we generated Figs 8 and 9 after an integration of these trajectories for 1000 h or >40 d. Here we choose four eccentricities compatible with an future observation mission ($e = 0$ up to $e = 0.3$). Largest eccentricities will hinder any accurate observation. Fig. 8 represents the maximum eccentricity reached by polar orbits in the anticlockwise direction. As we see, some orbits suffer less perturbations due to the irregular shape of (216) Kleopatra and mountain their eccentricity keep stable at a periapsis radius of 260 km for the circular case (Fig. 8a). Moreover, for obits with initial eccentricities (Figs 8b–d), this radius is same as the circular case (260 km). Below this value, most of the orbits will suffer major perturbation in the eccentricity and the tendency is that they escape. Scheeres et al. (2003) has shown that circular polar orbits can suffer eccentricity perturbations after 30 d and may escape. None the less, Figs 8(b) and (c) exhibit the fact that polar orbits with eccentricities ranging between 0.1 and 0.2 may be more stable. The behaviour of

Table 3. Number of initial conditions of polar orbits that impact or not with (216) Kleopatra for each initial periapsis radius (fist column) and eccentricities (second column).

Periapsis radius (km)	Initial eccentricity	Impact	Do not impact
Anticlockwise direction			
100	0	10	2
	0.1	10	2
	0.2	7	5
	0.3	6	6
140	0	8	4
	0.1	7	5
	0.2	6	6
	0.3	5	7
180	0	6	6
	0.1	2	10
	0.2	1	11
	0.3	0	12
220	0	1	11
	0.1	0	12
	0.2	0	12
	0.3	0	12
Clockwise direction			
100	0	10	2
	0.1	9	3
	0.2	7	5
	0.3	5	7
140	0	8	4
	0.1	10	2
	0.2	6	6
	0.3	7	5
180	0	6	6
	0.1	1	11
	0.2	1	11
	0.3	2	10
220	0	1	11
	0.1	0	12
	0.2	0	12
	0.3	0	12

the clockwise polar orbits is very similar (Fig. 9). Although these orbits seem to suffer slightly more perturbations from the irregular shape of (216) Kleopatra in the clockwise direction.

Now, we investigate the equatorial orbits that do not collide with the body after 1000 h, and the results are shown in Fig. 10. Fig. 10(a) confirms that all these orbits suffered perturbations in their initial eccentricities. The minimum radius for the circular case is 280 km despite significant perturbations of its orbit. A significant result shown in Fig. 10(c) is that stable orbits exist at a periapsis radius of 250 km for initial eccentricities $e = 0.2$. We investigated orbits closer than 250 km with higher eccentricities but we did not found any stable orbits. In view of the results for equatorial orbits, we show that the stable trajectories are closer for higher eccentricities, since the initial velocity is higher, especially here when the eccentricity reaches the value of 0.2. In this case, various orbits persist with the same initial eccentricity after 1000 h and possibly will continue stable. Two example of 3D orbits that remains stable around (216) Kleopatra after 1000 h are shown in Fig. 11. We take these examples to show that the perturbation of the gravitational potential of (216) Kleopatra disturbs the orbit making it to precess in both of cases. Being that the disturbance is higher for polar orbits. The initial eccentricity of these examples is 0.2 and their initial periapsis radius is 250 km.

6 CONCLUSIONS

In this paper, we used the mass of (216 Kleopatra) found by Descamps et al. (2011) and the density set by Carry (2012). The correction's factor of the Ostro et al. (2000) size was of 1.15. Thereby, we found values of the computed proprieties different than those reported by Yu & Baoyin (2012). These values were computed by effective algorithms (Mirtich 1996; Tsoulis 2012). We have shown that the behaviour of the zero-velocity curves differ substantially if we apply a scale size of 1.15 relative to the original shape of (216) Kleopatra. Therefore, the computation errors of the volume need to be corrected for further works on the dynamics of (216) Kleopatra. From the pseudo-potential, we also found the location of all the equilibrium points and their respective Jacobi constant. Regarding the inner points of (216) Kleopatra in Table 2, the equilibrium point $E6$ located at the centre of the body is unstable while the other two inner equilibrium points $E5$ and $E7$ are both linearly stable. It can indicate that 216 Kleopatra is less stable and it may suffer structural failure in the future (Hirabayashi & Scheeres 2014). An important point of our study of stability against impact is that the minimum radii are more suited than the maximum radii shown by Scheeres et al. (2000, 2003). Here we have investigated the dynamics of equatorial and polar orbits for three-dimensional motion close to (216) Kleopatra taking into account the initial eccentricity of the orbits. We found that the minimum radius for direct, equatorial circular orbits that will not impact with (216) Kleopatra surface is 300 km and the lower limit on radius for polar circular orbits is 240 km. The most significant results are that the stable orbits occur at 280 km for equatorial circular orbits despite significant perturbations of its orbit and stable orbits exist at a periapsis radius of 250 km for initial eccentricities $e_i = 0.2$ in both of cases. Being that the polar orbits with eccentricities ranging between 0.1 and 0.2 appear to be more stable. In fact, we have shown that there are stable orbits with initial eccentricities and do not suffer many perturbations than circular orbits. In this way, various orbits persist with a very small variation of the initial eccentricity after 1000 h and possibly will remain stable. Finally, from the results, the lower limit on radius for polar and equatorial orbits that remain stable around (216) Kleopatra seem to be the same. We can conclude that the line integrals of a homogeneous arbitrary shaped polyhedral source to evaluate the gravitational potential function well suit the irregular shape of (216) Kleopatra (as shown in Fig. 3) and should be taken into account near the body. It is reasonable to assume that the mass is homogeneous. However, it does not have to be true for a real asteroid. Recent observation of Asteroid (21) Lutetia, approached by the *Rosetta* spacecraft on 2010 July 10, showed that objects larger than 100–120 km in diameter are remnants of the primordial asteroidal distribution analysing its surface composition and temperature (Coradini et al. 2011). Moreover, its low mass and high density (Patzold et al. 2011) reveals that asteroid (21) Lutetia might have a dense metal-rich core. That leads us to the end of the Jupiter planet formation. The formation of a second generation of planetesimals may be triggered by the presence of a high-mass planet (Ayliffe et al. 2012). The dense layers of pebbles trapped by the gas density gap may have collapsed to form the core of planetesimals. In Chanut, Winter & Tshuchida (2013), we showed the mechanism of this capture and found that a planet on an eccentric orbit interact with the pebble layer formed by these resonances. Collisions occur and become important for a planetary eccentricity near Jupiters actual value. So it leads us to believe that (216) Kleopatra may have suffered great collisions, but its dense metal core has allowed not to be broken and could explain its present form. Certainly, this would

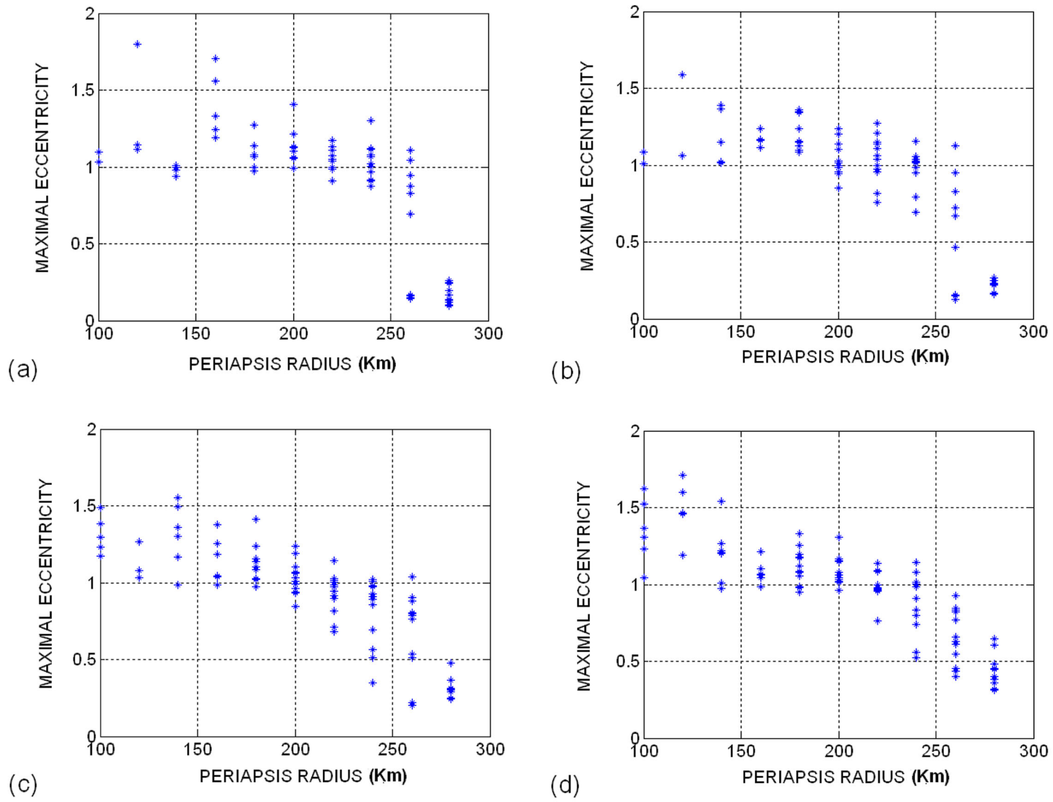

Figure 8. Maximal eccentricity of the polar anticlockwise orbits of the particles relative to (216) Kleopatra after 1000 h. The initial eccentricity *e* at their periapsis radius is (a) 0, (b) 0.1, (c) 0.2 and (d) 0.3.

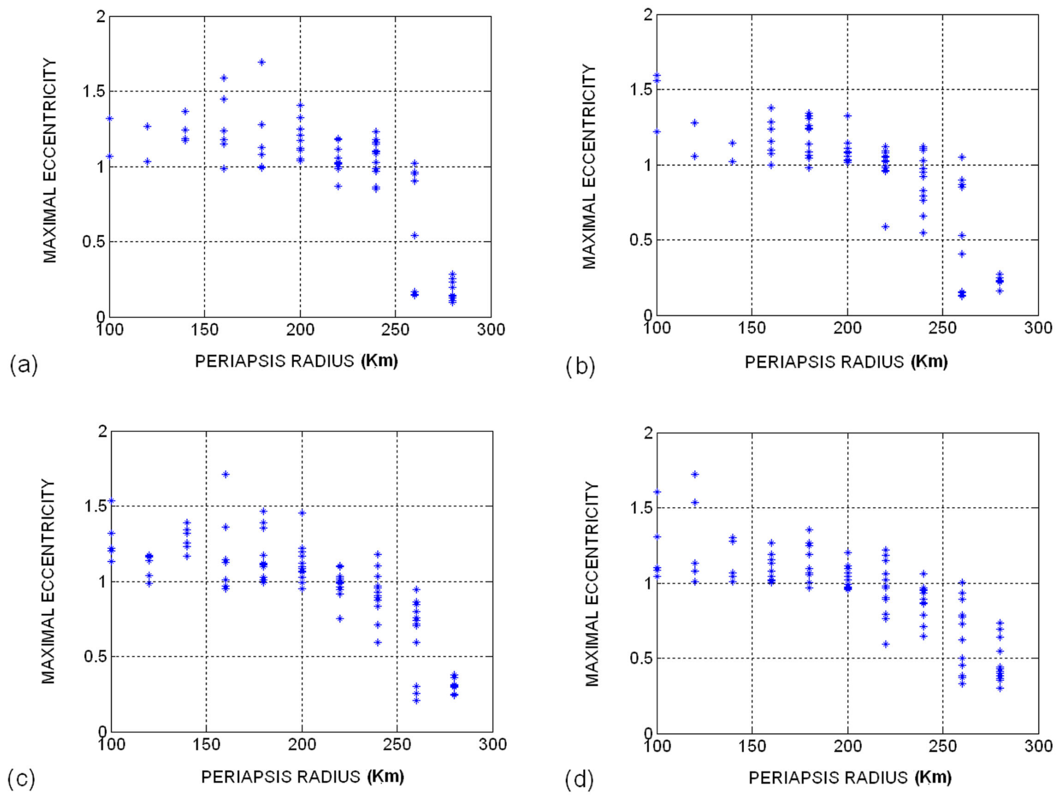

Figure 9. Maximal eccentricity of the polar clockwise orbits of the particles relative to (216) Kleopatra after 1000 h. The initial eccentricity *e* at their periapsis radius is (a) 0, (b) 0.1, (c) 0.2 and (d) 0.3.

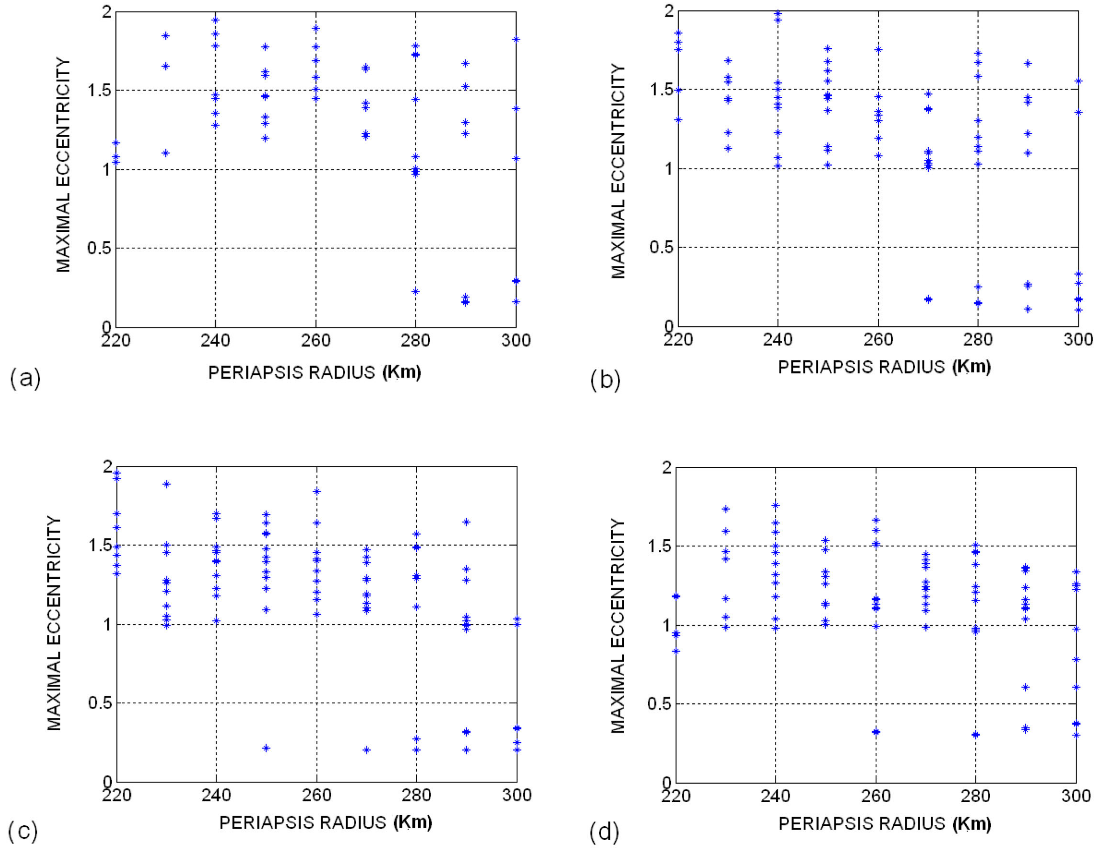

Figure 10. Maximal eccentricity of the equatorial orbits of the particles relative to (216) Kleopatra after 1000 h. The initial eccentricity e at their periapsis radius is (a) 0, (b) 0.1, (c) 0.2 and (d) 0.3.

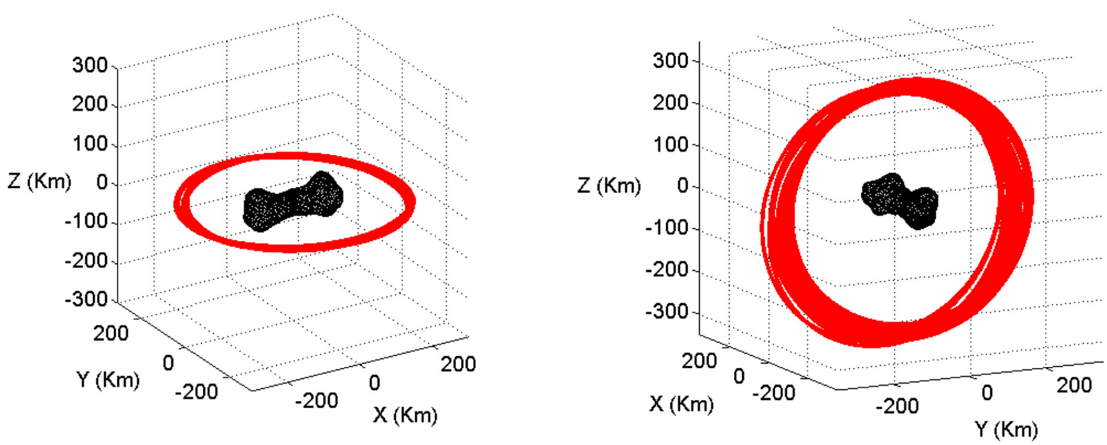

Figure 11. Examples of 3D orbit that remain stables around (216) Kleopatra after 1000 h. The initial eccentricity is 0.2 and the initial periapsis radius is 250 km for the both.

not be the only formation scenario but whatever if the actual friction angle of the partial volume of the neck is lower than the minimal friction angle (32° for asteroid's porosity of 44 per cent), the partial volume should fail when the size scale is 1.15 (Hirabayashi & Scheeres 2014). In this sense, we should expect a lower porosity of the neck of (216) Kleopatra. On the other hand, the classical polyhedron method needs a very large computational effort making a division into different layers impracticable. A solution would be to apply the new approach of the mascon gravitation (Chanut, Aljbaae & Carruba 2015) with a core–mantle discrimination and discuss the effect of different mass distributions. It is beyond the scope of this study and will be attempted in a future paper.

ACKNOWLEDGEMENTS

This work was supported by CAPES, CNPq, INCT - Estudos do Espaço and Fapesp proc. 2011/08171-3.

REFERENCES

Ayliffe B. A., Laibe G., Price D. J., Bate M. R., 2012, MNRAS, 423, 1450
Carry B., 2012, Planet. Space Sci., 73, 98
Chanut T. G. G., Winter O. C., Tshuchida M., 2013, A&A, 552, A66
Chanut T. G. G., Winter O. C., Tshuchida M., 2014, MNRAS, 438, 2672
Chanut T. G. G., Aljbaae S., Carruba V., 2015, MNRAS, 450, 3742
Coradini A. et al., 2011, Science, 334, 492
Descamps P. et al., 2011, Icarus, 211, 1022
Dobrovolskis A. R., 1996, Icarus, 124, 698
Harris A. W., 1998, Icarus, 131, 291
Hirabayashi M., Scheeres D. J., 2014, ApJ, 780, 160
Hu W., Scheeres D. J., 2004, Planet. Space Sci., 52, 685
Hussmann H., Oberst J., Wickhusen K., Shi X., Damme F., Lüdicke F., Lupovka V., Bauer S., 2012 Planet. Space Sci., 70, 102
Jiang Y., Baoyin H., Li J., Li H., 2014, Astrophys. Space Sci., 349, 83
Lebofsky L. A., Spencer J., 1989, in Binzel R. P., Gehrels T., Matthews M. S., eds, Asteroids II. Univ. Arizona Press, Tucson, AZ, p. 128
Magnusson P., 1990, Icarus, 85, 229
Mirtich B., 1996, J. Graph. Tools, 1, 2
Mitchell J. K., Houston W. N., Scott R. F., Costes N. C., Carrier W. D., III, Bromwell L. G., 1972, Proc. Lunar Planet. Sci. Conf., 3, 3235
Ostro S. J., Campbell D. B., Shapiro I. I., 1985, Science, 229, 442
Ostro S. J. et al., 2000, Science, 288, 836
Patzold M. et al., 2011, Science, 334, 491
Rossi A., Marzari F., Farinella P., 1999, Earth Planets Space, 51, 1173
Ryan E. L., Woodward C. E., 2010, AJ, 140, 933
Scheeres D. J., 1994, Icarus, 110, 225
Scheeres D. J., Ostro S. J., Hudson R. S., Werner R. A., 1996, Icarus, 121, 67
Scheeres D. J., Ostro S. J., Hudson R. S., DeJong E. M., Suzuki S., 1998, Icarus, 132, 53
Scheeres D. J., Williams B. G., Miller J. K., 2000, J. Guid. Control Dyn., 23, 466
Scheeres D. J., Miller D. K., Yeomans J. K., 2003, The Orbital Dynamics environment of 433 Eros: A case study for future missions, IPN Progress Report, 42, 1
Scheeres D. J. et al., 2006, Proc. AIAA/AAS Astrodyn. Specialist Conf. and Exhibit, AIAA Paper 2006–6661, The Actual Dynamical Environment About Itokawa, Keystone, Colorado, p. 21
Scott R. F., 1963, Principles of Soil Mechanics. Addison-Wesley, Boston, MA
Tedesco E. F., Noah P. V., Noah M., Price S. D., 2002, AJ, 123, 1056
Tsoulis D., 1999, Deutsche Geodätische Kommission, Reihe C, Heft Nr 510 Vaticana Ric. Astron., 6, 341
Tsoulis D., 2012, Geophysics, 77, F1
Tsoulis D., Petrović S, 2001, Geophysics, 66, 535
Werner R. A., Scheeres D. J., 1997, Celest. Mech., 65, 313
Yu Y., Baoyin H., 2012, AJ, 143, 62
Yu Y., Baoyin H., 2013, Ap&SS, 343, 74

This paper has been typeset from a TEX/LATEX file prepared by the author.